Chinese Chemical Letters 37 (2026) 112817

Contents lists available at ScienceDirect

Chinese Chemical Letters

journal homepage: www.elsevier.com/locate/cclet

Thiazole-linked pyrene covalent organic framework for selective sulfoxidation *via* an electron transfer mediator by photoredox catalysis

Min Hou, Yuexin Wang*, Siyu Zhang, Keke Zhang, Xiu Tan, Xianjun Lang*

Hubei Key Lab on Organic and Polymeric Optoelectronic Materials, College of Chemistry and Molecular Sciences, Wuhan University, Wuhan 430072, China

ARTICLE INFO

Article history:
Received 7 January 2026
Revised 9 April 2026
Accepted 21 April 2026
Available online 23 April 2026

Keywords:
Covalent organic frameworks
Thiazole linkage
Tempo
Electron transfer
Aerobic sulfoxidation

ABSTRACT

Covalent organic frameworks (COFs) are burgeoning for visible-light photoredox catalysis owing to their modular building blocks and convertible covalent linkages. Herein, the polycondensation of 1,3,6,8-tetra(4-formylphenyl)pyrene (Py) and 4,4′-biphenyldiamine (BD) affords an imine-linked COF, PyBD-COF. Consequently, the conversion of imine into thiazole yields a thiazole-linked COF, PyBTZ-COF. Both pyrene COFs possess well-defined crystallinity and porosity. Compared to PyBD-COF, PyBTZ-COF exhibits superior chemical stability and better electronic structure, attributable to its stable and photoactive thiazole linkages. Both PyBD-COF and PyBTZ-COF drive highly selective sulfoxidation by blue-light photoredox catalysis. Notably, 3 mol% TEMPO (2,2,6,6-tetramethylpiperidine-*N*-oxyl) as electron transfer mediator enhances the conversions to approximately twofold for both PyBD-COF and PyBTZ-COF compared to TEMPO-free conditions. Due to its better electronic structure, PyBTZ-COF outperforms PyBD-COF for selective aerobic sulfoxidation, irrespective of addition of 3 mol% TEMPO. PyBTZ-COF photoredox catalysis with TEMPO exhibits excellent stability and broad applicability for selective sulfoxidation. The conversion of the linkage of COFs offers a way forward for enhancing performance in photoredox catalysis.

© 2026 Published by Elsevier B.V. on behalf of Chinese Chemical Society and Institute of Materia Medica, Chinese Academy of Medical Sciences.

As burgeoning crystalline porous materials, covalent organic frameworks (COFs) possess an inherent porosity, ordered π-conjugation, and tunable structure [1–3]. These properties endow them with considerable potential for visible-light photoredox catalysis, such as hydrogen peroxide production [4], carbon dioxide reduction [5], hexavalent chromium reduction [6,7], and selective organic conversion [8]. COFs are constructed from modular organic building blocks connected by covalent linkages [9]. The linkage significantly influences the attributes of COFs [10]. Notably, over 60 % of all COFs are linked by the imine linkage [11], as the reversibility of the imine linkage enables smooth synthesis that imparts high crystallinity under mild conditions [12,13]. However, this reversibility of the imine linkage adversely affects the structural stability, and the inherent polarization results in π-electron delocalization [14]. It is imperative to address these intrinsic limitations of imine-linked COFs to exploit their full potential in photoredox catalysis. A sustainable solution is the conversion of the imine linkage to afford highly stable COFs with extended π-conjugation [15–17]. Compared to the imine linkage, the rigid thiazole linkage can confer enhanced structural stability to COFs [18,19], enabling their stability in photoredox catalysis. In parallel, due to the differences in atomic size and electronegativity between C and S, the electronic structure of COFs can be modulated by the incorporation of S [20]. Furthermore, as a heterocyclic aromatic ring, thiazole features a delocalized π-electron system, which facilitates photogenerated electron transfer in thiazole-linked COFs [21]. Taken together, the conversion of imine into thiazole is viable to enhance the chemical stability and local electronic structure of COFs.

Following the selection of a suitable linkage, the choice of building blocks for knots is equally crucial, as it dictates both the fundamental architecture and electronic structure of the COFs [22]. Pyrene, a polycyclic aromatic hydrocarbon, serves as a prominent chromophore with exceptional light-harvesting capability [23]. Moreover, its extensive planar π-conjugated structure allows efficient photogenerated charge separation and transfer [24]. Owing to these merits, pyrene and its derivatives are among the most attractive knots for COFs. To date, pyrene COFs play a pivotal role in diverse fields, such as organic optoelectronics and proton conduction [25,26]. Of particular note, pyrene COFs have exhibited exceptional performance in photoredox catalysis [27].

The performance of COF is frequently constrained by charge carrier recombination [28]. This limitation can be effectively addressed *via* an electron transfer mediator. During photoredox catalysis, electron transfer, typically the rate-determining step, is accel-

* Corresponding authors.
E-mail addresses: yuexinwang@whu.edu.cn (Y. Wang), xianjunlang@whu.edu.cn (X. Lang).

https://doi.org/10.1016/j.cclet.2026.112817
1001-8417/© 2026 Published by Elsevier B.V. on behalf of Chinese Chemical Society and Institute of Materia Medica, Chinese Academy of Medical Sciences.

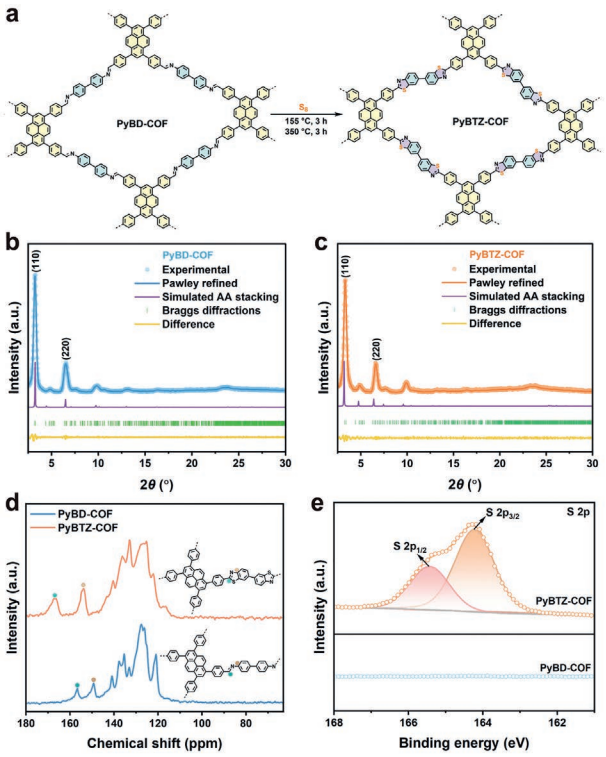


Fig. 1. (a) Schematic illustration of the conversion from PyBD-COF to PyBTZ-COF. Experimental, simulated, and Pawley refined PXRD patterns of PyBD-COF (b) and PyBTZ-COF (c). Solid-state ^{13}C NMR spectra (d), and high-resolution XPS spectra of S 2p (e) of PyBD-COF and PyBTZ-COF.

erated by the use of mediators [29–31]. A stable organic nitroxyl radical TEMPO (2,2,6,6-tetramethylpiperidine-*N*-oxyl) can be used as an electron transfer mediator in organic conversions [32]. As is well known, organic sulfoxides are essential compounds that are extensively utilized in organic synthesis [33]. Selective sulfoxidation to value-added sulfoxides is feasible by photoredox catalysis [34,35]. Notably, TEMPO has successfully accelerated the oxidation of sulfides by COF photoredox catalysis [36]. Considering these factors, pyrene COFs can be more promising for selective aerobic sulfoxidation *via* TEMPO.

Herein, the polycondensation of 1,3,6,8-tetra(4-formylphenyl)pyrene (Py) and 4,4′-biphenyldiamine (BD) affords an imine-linked COF, PyBD-COF, according to a prior report [37]. Subsequently, the conversion of imine into thiazole yields a thiazole-linked COF, PyBTZ-COF (Fig. 1a). Intriguingly, attributable to its stable and photoactive thiazole linkage, PyBTZ-COF exhibits superior chemical stability and better electronic structure compared to PyBD-COF. Both PyBD-COF and PyBTZ-COF drive highly selective sulfoxidation by blue-light photoredox catalysis. Notably, with the addition of 3 mol% TEMPO as an electron transfer mediator, for both COFs, the conversions increased to approximately twofold compared to TEMPO-free conditions. Owing to its better electronic structure, PyBTZ-COF outperforms PyBD-COF for selective sulfoxidation, irrespective of addition of 3 mol% TEMPO. Substrate scope and recycling reveal that PyBTZ-COF photoredox catalysis possesses broad applicability and excellent stability for selective sulfoxidation *via* TEMPO.

First, the powder X-ray diffraction (PXRD) patterns of PyBD-COF and PyBTZ-COF confirm their well-defined crystallinity (Figs. 1b and c). The diffraction peaks at 3.25° for PyBD-COF and 3.29° for PyBTZ-COF correspond to the (110) planes. The shift of the main peak to a higher angle results from the oxidative cyclization of imine into thiazole [38]. Additionally, the minimal Pawley refinement residue values ($R_{wp} = 6.16$ %, $R_p = 4.59$ %) for PyBD-COF and ($R_{wp} = 4.86$ %, $R_p = 3.67$ %) for PyBTZ-COF demonstrate that the experimental PXRD patterns are consistent with the simulated AA stackings (Fig. S1, Tables S3 and S4 in Supporting information).

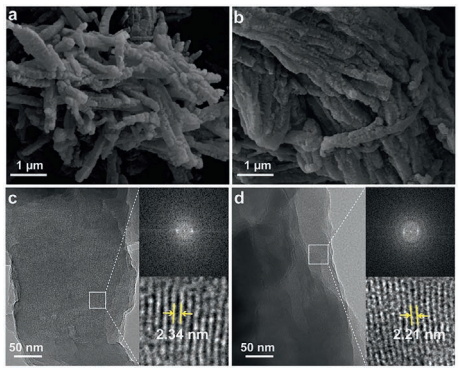


Fig. 2. SEM images of PyBD-COF (a) and PyBTZ-COF (b). TEM images of PyBD-COF (c) and PyBTZ-COF (d).

Next, Fourier transform infrared (FTIR) and solid-state ^{13}C nuclear magnetic resonance (NMR) spectra illuminate the chemical structures of both PyBD-COF and PyBTZ-COF. The emergence of the C=N stretching vibration at 1620 cm^{-1} indicates the successful formation of PyBD-COF (Fig. S2 in Supporting information). In contrast, this peak disappeared in PyBTZ-COF, and a new peak at 1603 cm^{-1} appeared, which is attributed to the formation of the thiazole linkage [39]. As shown in Fig. 1d, the imine C signal appears at 156.7 ppm in PyBD-COF, whereas it shifts to 167.1 ppm in PyBTZ-COF. Additionally, the chemical shift of the C adjacent to the imine N changed from 149.2 ppm in PyBD-COF to 153.9 ppm in PyBTZ-COF, suggesting the conversion of imine into thiazole [40,41]. Furthermore, X-ray photoelectron spectroscopy (XPS) was applied to verify the conversion. The XPS survey spectra of PyBD-COF and PyBTZ-COF display C 1s, N 1s, and O 1s peaks, whereas the spectrum of PyBTZ-COF exhibits additional distinct S 2s and S 2p peaks (Fig. S3a in Supporting information). The high-resolution S 2p spectrum of PyBTZ-COF shows two peaks at 164.2 eV ($2p_{3/2}$) and 165.4 eV ($2p_{1/2}$). The positive shift of S $2p_{3/2}$ peak in PyBTZ-COF compared to that of S_8 (164.0 eV) confirms the formation of the thiazole linkage (Fig. 1e) [18]. This conclusion is further corroborated by the concomitant shift of the N 1s peak from 399.0 eV in PyBD-COF to 399.1 eV in PyBTZ-COF (Fig. S3b in Supporting information).

Furthermore, the porosity was evaluated from N_2 adsorption–desorption isotherms (Figs. S4a and b in Supporting information). A typical type IV isotherm was observed for both pyrene COFs. Notably, the Brunauer–Emmett–Teller (BET) specific surface area of PyBTZ-COF (625 m^2/g) was even higher than that of PyBD-COF (575 m^2/g). Nonlocal density functional theory (DFT) calculations showed dominant pore sizes of 2.16 nm for PyBD-COF and 2.00 nm for PyBTZ-COF (Figs. S4c and d in Supporting information), which closely match the values derived from their simulated crystal structures (Figs. S4e and f in Supporting information).

Besides, the morphological features of PyBD-COF and PyBTZ-COF were probed by scanning electron microscopy (SEM) and transmission electron microscopy (TEM). The SEM images reveal that both COFs exhibited analogous rod morphologies with micron length (Figs. 2a and b). Distinct lattice fringes were observed in TEM images, demonstrating high crystallinity of both COFs (Figs. 2c and d). Furthermore, the elemental mappings reveal a homogeneous distribution of S in PyBTZ-COF (Fig. S5 in Supporting information). Additionally, elemental analysis further verified the suc-

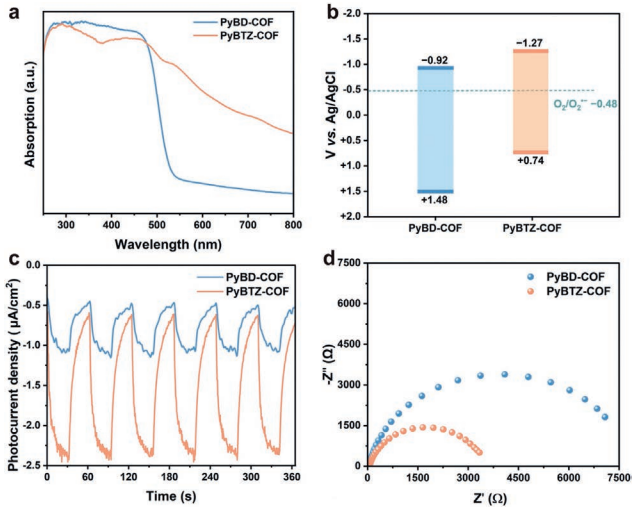


Fig. 3. UV–vis DRS (a), band structures (b), transient photocurrent densities (c), and EIS Nyquist plots (d) of PyBD-COF and PyBTZ-COF.

cessful construction of PyBD-COF and PyBTZ-COF (Table S1 in Supporting information).

The chemical stability of PyBD-COF and PyBTZ-COF was evaluated by exposing them to harsh conditions, including strong acid (6 mol/L HCl), strong base (6 mol/L NaOH), and reducing agent (1 mol/L $NaBH_4$) for 12 h. PyBTZ-COF maintained its crystallinity, whereas PyBD-COF exhibited severe structural damage, according to the PXRD patterns (Figs. S6a and b in Supporting information). Additionally, the FTIR spectra show significant changes in the C=N stretching vibration in PyBD-COF, while that of PyBTZ-COF remained unchanged, confirming its structural stability (Figs. S6c and d in Supporting information). Besides, thermogravimetric analysis (TGA) curves show that the decomposition temperature of PyBTZ-COF is higher than that of PyBD-COF (Fig. S7 in Supporting information). These results indicate that PyBTZ-COF exhibited enhanced stability compared to PyBD-COF, thereby broadening its potential under diverse operational conditions.

The optoelectronic properties of PyBD-COF and PyBTZ-COF were further investigated. The ultraviolet–visible diffuse reflectance spectroscopy (UV–vis DRS) spectra exhibit a significant enhancement in the optical absorption of PyBTZ-COF compared to PyBD-COF across the 500–800 nm spectral range (Fig. 3a). Compared to its building blocks, PyBTZ-COF exhibited a significantly enhanced absorption in the visible region (Fig. S8 in Supporting information). Additionally, the band gaps (E_g) of PyBD-COF and PyBTZ-COF were calculated as 2.40 and 2.01 eV, respectively (Fig. S9 in Supporting information). The narrower E_g in PyBTZ-COF is due to the extended π-conjugation from its thiazole linkage. Besides, the Mott–Schottky plots show positive slopes for PyBD-COF and PyBTZ-COF, indicating that they are n-type semiconductors (Fig. S10 in Supporting information). Based on the flat band potentials relative to the lowest unoccupied molecular orbital (LUMO) level of the n-type semiconductor [42], for PyBD-COF and PyBTZ-COF, the LUMO level was measured to be −0.92 and −1.27 V (*vs.* Ag/AgCl), respectively. These values confirm that both COFs can thermodynamically drive the reduction of O_2 to superoxide radical anion ($O_2^{\bullet-}$) [43]. Additionally, the highest occupied molecular orbital (HOMO) levels of PyBD-COF and PyBTZ-COF were calculated as +1.48 and +0.74 V, respectively (Fig. 3b). Subsequently, photoelectrochemical characterizations were conducted to assess the charge separation and transfer of PyBD-COF and PyBTZ-COF. PyBTZ-COF exhibited higher photocurrent density than PyBD-COF (Fig. 3c), suggesting more efficient charge separation and transfer. This conclusion is further

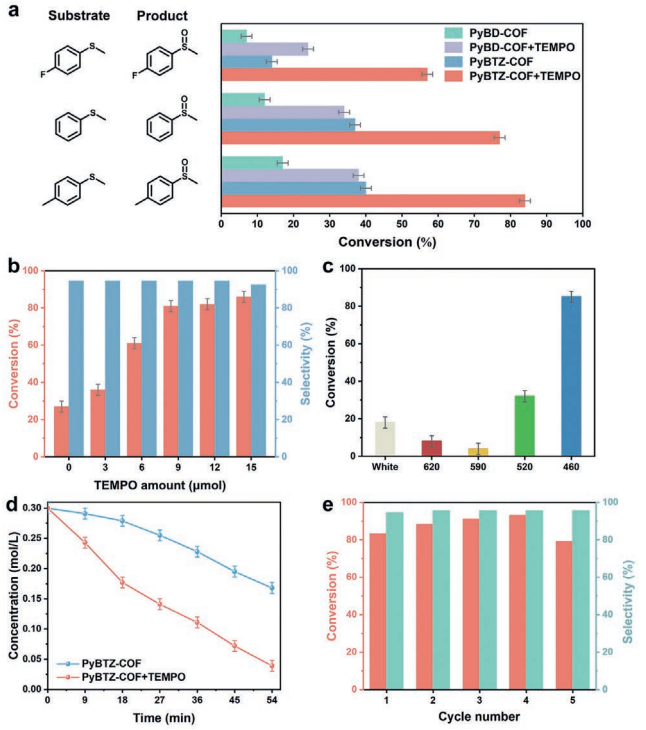


Fig. 4. (a) The conversion comparison of sulfoxidation with or without 3 mol% TEMPO for PyBD-COF and PyBTZ-COF by photoredox catalysis. (b) The effect of TEMPO amount on sulfoxidation by PyBTZ-COF photoredox catalysis. (c) The impact of LED wavelength on sulfoxidation *via* TEMPO by PyBTZ-COF photoredox catalysis. (d) Kinetic curves of sulfoxidation with or without 3 mol% TEMPO by PyBTZ-COF photoredox catalysis. (e) Recycling experiments on sulfoxidation *via* TEMPO by PyBTZ-COF photoredox catalysis. Reaction conditions: COF (4 mg), organic sulfide (0.3 mmol), blue LEDs, CH_3OH (1 mL), O_2 (0.1 MPa). Reaction time: (a), (b), and (e) 50 min; (c) 60 min.

corroborated by electrochemical impedance spectroscopy (EIS) results (Fig. 3d), where PyBTZ-COF displayed a smaller arc radius in the Nyquist plot. Under visible-irradiation, electron (e^-) and hole (h^+) can be produced over PyBD-COF and PyBTZ-COF to carry out their respective redox reactions.

Next, the performance of PyBD-COF and PyBTZ-COF for sulfoxidation was examined under the irradiation of 460 nm blue light-emitting diodes (LEDs, Fig. 4a). Both PyBD-COF and PyBTZ-COF photoredox catalysis drove the highly selective sulfoxidation. PyBTZ-COF outperformed PyBD-COF, exhibiting significantly higher conversion, which may be attributed to the better electronic structures. Notably, the addition of 3 mol% TEMPO enhanced the conversions of organic sulfide for both PyBD-COF and PyBTZ-COF to approximately twofold compared to the TEMPO–free conditions. This result indicates that the use of a catalytic amount of TEMPO effectively accelerates selective sulfoxidation for both pyrene COFs. Given the superior performance of PyBTZ-COF, a detailed investigation was further conducted for sulfoxidation *via* TEMPO by photoredox catalysis.

The effect of TEMPO loading on sulfoxidation was systematically investigated (Fig. 4b). Increasing the TEMPO amount from 1 mol% to 3 mol% significantly enhanced the conversion of methyl phenyl sulfide, whereas further increases beyond 3 mol% yielded only marginal improvements. Additionally, the impact of LED wavelength on selective sulfoxidation *via* TEMPO by PyBTZ-COF photoredox catalysis was explored (Fig. 4c). The results indicate that the conversions of methyl phenyl sulfide were relatively low under the irradiation of white LEDs, as well as 620, 590, and 520 nm LEDs. In contrast, superior performance was observed under the irradiation of blue LEDs. In light of the performance, blue LEDs

were chosen as the standard light source for subsequent investigations. To gain a deeper insight, comprehensive kinetic studies were performed (Fig. 4d). Analysis of the time-concentration profiles reveals that TEMPO significantly enhanced the conversion of methyl phenyl sulfide by photoredox catalysis. Besides, the performance of the building blocks was much lower than that of PyBTZ-COF, regardless of TEMPO addition (Table S2 in Supporting information). Recycling experiments were further carried out (Fig. 4e). Over five cycles, no significant decrease in conversion was observed for PyBTZ-COF, confirming that it retained high performance across multiple runs. Importantly, PXRD and SEM results confirm that the recycled PyBTZ-COF retained its crystallinity and morphological features, and negligible changes were observed in the FTIR spectra (Figs. S11–S13 in Supporting information), demonstrating the excellent stability of PyBTZ-COF during photoredox catalysis.

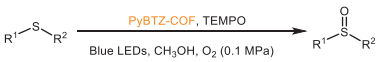
Subsequently, the substrate scope was examined for selective sulfoxidation *via* TEMPO by PyBTZ-COF photoredox catalysis. As presented in Table 1, various organic sulfides were converted to the corresponding sulfoxides with high conversions and selectivities, demonstrating the broad applicability. Under comparable conversions, methyl phenyl sulfides bearing electron-donating groups at the *para*-position required lesser reaction time (Table 1, entries 1–3), whereas those bearing electron-withdrawing substituted groups at the *para*-position necessitated longer reaction durations (Table 1, entries 4–7). These results highlight the pronounced influence of electronic effects on the conversion and selectivity of the sulfoxidation reaction. The conversion was also influenced by the position of the substituent on the phenyl ring. For the −Cl substituent, the reaction rate followed the order *ortho* < *meta* < *para* (Table 1, entries 5, 8, and 9), whereas the $-OCH_3$ group displayed a different trend with *meta* < *ortho* < *para* (Table 1, entries 3, 10, and 11). Furthermore, replacing the methyl group in methyl phenyl sulfide with an ethyl group, or substituting the phenyl ring with a naphthyl group, prolonged the reaction time needed to achieve comparable conversion (Table 1, entries 1, 12, and 13). These results underscore the significant role of steric hindrance in governing the conversion. Moreover, aliphatic sulfides reached high conversions in much shorter reaction time compared to phenyl sulfides (Table 1, entries 14 and 15).

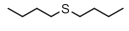
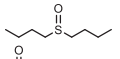
Control and quenching experiments were performed to elucidate the mechanism of selective sulfoxidation *via* TEMPO by PyBTZ-COF photoredox catalysis (Fig. 5a). Notably, no reaction occurred in the dark, demonstrating that blue light was indispensable. Furthermore, the conversion decreased significantly upon the addition of $AgNO_3$ (e^- scavenger) and KI (h^+ scavenger), respectively. Thus, the involvements of both e^- and h^+ was confirmed. Typically, reactive oxygen species (ROS) are pivotal for photoredox catalysis [44,45]. The reaction was inhibited in air and completely suppressed under an N_2 atmosphere, implying that O_2 is essential for ROS generation. Moreover, the conversion decreased significantly upon quenching of $O_2^{\bullet-}$ by *p*-benzoquinone (*p*-BQ). In contrast, introducing CD_3OD, which prolongs the lifetime of singlet oxygen ($^1O_2$) [46], did not cause a noticeable change, indicating that $O_2^{\bullet-}$, not $^1O_2$, is the key ROS. Subsequently, the effect of O_2 pressure was investigated (Fig. S14 in Supporting information). As the O_2 pressure increased, the conversion of methyl phenyl sulfide gradually increased and eventually plateaued after 0.3 MPa.

Electron paramagnetic resonance (EPR) spectroscopy was adopted to verify the conclusion. The e^- signal continuously increased under sustained light irradiation and then sharply decreased upon exposure to O_2, indicating e^- is consumed to form $O_2^{\bullet-}$ (Fig. 5b). Furthermore, 5,5-dimethyl-1-pyrroline *N*-oxide (DMPO) was employed to capture $O_2^{\bullet-}$. The gradual enhancement of DMPO–$O_2^{\bullet-}$ signals with prolonged illumination time confirmed $O_2^{\bullet-}$ as the key ROS (Fig. 5c). TEMPO is a stable radical that can be directly detected by EPR spectra [47]. A distinct signal of TEMPO was clearly detected under dark conditions, weakened under irradiation, and then recovered in the dark (Fig. 5d). This indicates a reversible conversion between TEMPO (EPR-active) and $TEMPO^+$ (EPR-silent) during the reaction. Furthermore, DFT calculations were used to analyze the local electronic structure of PyBTZ-COF (Fig. 5e). The HOMO is primarily located at the pyrene unit, while the LUMO is delocalized at the pyrene and benzothiazole units. These results indicate that PyBTZ-COF enables effective electron transfer from the pyrene to the benzothiazole unit upon photoexcitation.

Guided by the above results, a reaction mechanism is proposed for selective sulfoxidation *via* TEMPO by PyBTZ-COF photoredox catalysis (Fig. 5f). Firstly, under the irradiation of blue LEDs, the photoexcited PyBTZ-COF produces e^- and h^+. Subsequently, O_2 is reduced to $O_2^{\bullet-}$ by e^-, while TEMPO is oxidized to $TEMPO^+$ by h^+. $TEMPO^+$ further reacts with methyl phenyl sulfide, converting it into a sulfur radical cation. Lastly, the sulfur radical cation

Table 1
The substrate scope for selective sulfoxidation *via* TEMPO by PyBTZ-COF photoredox catalysis.[a]



Entry	Substrate	Product	*t* (min)	Conversion (%)[b]	Selectivity (%)[b]
1			65	89	99
2			55	93	99
3			55	99	99
4			90	91	99
5			95	89	98
6			95	95	97
7			95	89	98
8			155	89	99
9			205	96	99
10			75	90	99
11			75	95	99
12			70	90	98
13			115	92	97
14			21	95	99
15			20	98	99

[a] Reaction conditions: PyBTZ-COF (4 mg), TEMPO (3 mol%), organic sulfide (0.3 mmol), blue LEDs, CH_3OH (1 mL), O_2 (0.1 MPa).
[b] Detected by GC–FID.

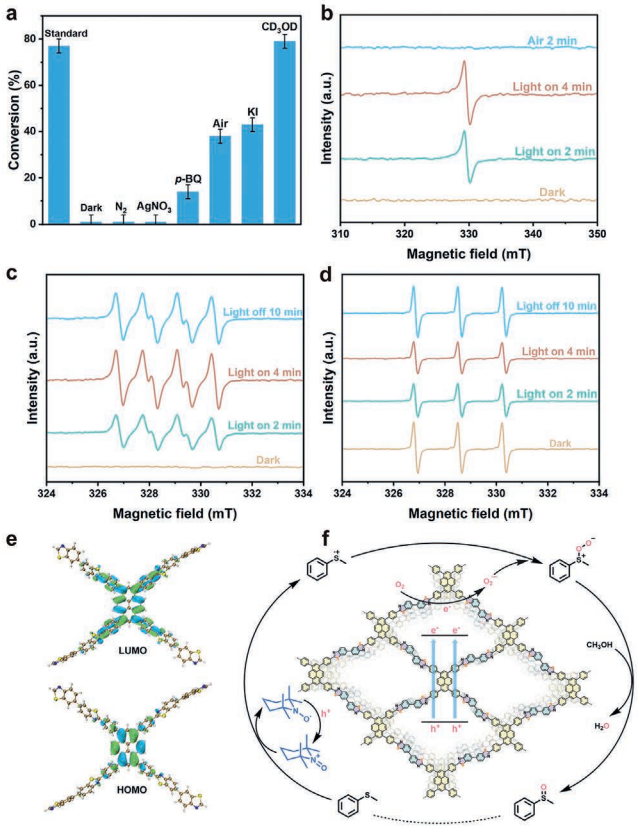


Fig. 5. (a) Control and quenching results for selective sulfoxidation. The EPR spectra of e^- (b), DMPO trapped $O_2^{\bullet-}$ (c), and TEMPO (d). (e) The HOMO and LUMO distributions of the simplified structural fragments of PyBTZ-COF. (f) A proposed reaction mechanism for selective sulfoxidation *via* TEMPO by PyBTZ-COF photoredox catalysis. Reaction conditions: PyBTZ-COF (4 mg), methyl phenyl sulfide (0.3 mmol), blue LEDs, CH_3OH (1 mL), O_2 (0.1 MPa), 50 min.

combines with $O_2^{\bullet-}$ to afford methyl phenyl persulfoxide, which is converted into methyl phenyl sulfoxide *via* proton and electron donations by CH_3OH.

In summary, the polycondensation of Py and BD has afforded an imine-linked COF, PyBD-COF, which was further converted into a thiazole–linked COF PyBTZ–COF *via* linkage conversion. Intriguingly, the stable and photoactive thiazole linkage in PyBTZ-COF endowed it with superior chemical stability and better electronic structure compared to PyBD-COF. Both COFs achieved highly selective sulfoxidation by blue-light photoredox catalysis. Importantly, 3 mol% TEMPO as electron transfer mediator enhanced the conversions to approximately twofold for both PyBD-COF and PyBTZ-COF compared to TEMPO-free conditions. Due to its better electronic structure, PyBTZ-COF outperformed PyBD-COF for blue-light photoredox catalysis. PyBTZ-COF exhibited excellent stability and broad applicability for selective sulfoxidation *via* TEMPO. The linkage conversion can effectively optimize the local electronic structure of COFs, thereby enhancing photoredox catalysis.

Declaration of competing interest

The authors declare that they have no known competing financial interests or personal relationships that could have appeared to influence the work reported in this paper.

CRediT authorship contribution statement

Min Hou: Writing – original draft, Investigation, Formal analysis. **Yuexin Wang:** Writing – review & editing, Investigation, Formal analysis, Conceptualization. **Siyu Zhang:** Investigation, Formal analysis. **Keke Zhang:** Investigation, Formal analysis. **Xiu Tan:** Investigation, Formal analysis. **Xianjun Lang:** Writing – review & editing, Supervision, Funding acquisition, Conceptualization.

Acknowledgments

This work was supported by the National Natural Science Foundation of China (No. 22372124). The numerical calculations were done on the supercomputing system in the Supercomputing Center of Wuhan University. We also acknowledge the Core Facility of Wuhan University and the Center for Electron Microscopy at Wuhan University for materials characterizations.

Supplementary materials

Supplementary material associated with this article can be found, in the online version, at doi:10.1016/j.cclet.2026.112817.

References

[1] M.S. Lohse, T. Bein, Adv. Funct. Mater. 28 (2018) 1705553.
[2] X.R. Li, X.Y. Ji, X.L. Zhang, et al., Nat. Commun. 16 (2025) 1223.
[3] M. Asad, M.I. Anwar, A. Abbas, et al., Coord. Chem. Rev. 463 (2022) 214539.
[4] R.C. Chen, C.M. Wu, L.H. Chung, et al., Chem. Mater. 36 (2024) 9928–9938.
[5] H.X. Xu, W.Z. Wang, C. Liu, et al., Adv. Funct. Mater. 36 (2026) e15586.
[6] Y. Sun, J.E. Szulejko, K.H. Kim, et al., Chin. J. Catal. 55 (2023) 20–43.
[7] S.C. Zhong, Y. Wang, M.S. Xie, et al., Chin. Chem. Lett. 36 (2025) 110312.
[8] Z. Li, F.L. Zhang, H.X. Zhao, et al., J. Mater. Chem. A 13 (2025) 5169–5179.
[9] K.Y. Geng, T. He, R.Y. Liu, et al., Chem. Rev. 120 (2020) 8814–8933.
[10] X.B. Yang, Q. Xu, W. Wei, G.F. Zeng, Angew. Chem. Int. Ed. 64 (2025) e202504355.
[11] A. Volkov, J.S. Mi, K. Lalit, et al., J. Am. Chem. Soc. 145 (2023) 6230–6239.
[12] P.N. Anjana, A.K. Pulikkal, Microporous Mesoporous Mater. 387 (2025) 113516.
[13] C. Qian, L.L. Feng, W.L. Teo, et al., Nat. Rev. Chem. 6 (2022) 881–898.
[14] G.X. Jiang, W.W. Zou, Z.Y. Ou, et al., Chem. Eur. J. 29 (2023) 202203610.
[15] L. Cusin, H.J. Peng, A. Ciesielski, P. Samorì, Angew. Chem. Int. Ed. 60 (2021) 14236–14250.
[16] J.R. Wang, K.P. Song, T.X. Luan, et al., Nat. Commun. 15 (2024) 1267.
[17] Q.Y. Wang, J. Liu, M. Cao, et al., Angew. Chem. Int. Ed. 61 (2022) e202207130.
[18] K.W. Wang, Z.F. Jia, Y. Bai, et al., J. Am. Chem. Soc. 142 (2020) 11131–11138.
[19] M.J. Deng, J. Chakraborty, G.Z. Wang, et al., J. Am. Chem. Soc. 147 (2025) 10219–10230.
[20] R. Gutru, Z. Turtayeva, F.A. Xu, et al., Int. J. Hydrog. Energy 48 (2023) 3593–3631.
[21] X. Chi, Z.X. Zhang, M.Q. Li, et al., Angew. Chem. Int. Ed. 64 (2025) e202418895.
[22] Y.K. Liu, X.A. Liu, A. Su, et al., Chem. Soc. Rev. 53 (2024) 502–544.
[23] A. Garci, J.A. Weber, R.M. Young, et al., Nat. Catal. 5 (2022) 524–533.
[24] X.Y. Dong, H.X. Zhao, K.K. Zhang, X.J. Lang, Coord. Chem. Rev. 513 (2024) 215902.
[25] Z.W. Li, T. Tsuneyuki, R.P. Paitandi, et al., J. Am. Chem. Soc. 146 (2024) 23497–23507.
[26] J.H. Li, G.N. Chen, C.H. Chen, et al., Chin. Chem. Lett. 36 (2025) 109760.
[27] J. Cheng, Y. Wu, W. Zhang, et al., Adv. Mater. 36 (2024) 2305313.
[28] L. Wang, C.Z. Han, S.Y. Gao, et al., ACS Catal. 15 (2025) 5683–5693.
[29] H.B. Wu, F. Qi, L.J. Wang, et al., Adv. Energy Mater. 15 (2025) 2502285.
[30] X.W. Zhao, X.L. Bai, R. Zhai, et al., Appl. Catal. B 370 (2025) 125166.
[31] H.T. Wang, Y.Z. Shi, J.Y. Guo, et al., Chin. Chem. Lett. 36 (2025) 110779.
[32] F.W. Huang, F.L. Zhang, Y.X. Wang, X.J. Lang, Trends Chem. 6 (2024) 115–127.
[33] P. Ran, M.Z. Sun, A.Q. Qiu, et al., J. Am. Chem. Soc. 143 (2025) 26254–26266.
[34] F.L. Zhang, Y.X. Wang, H.X. Zhao, et al., ACS Appl. Mater. Interfaces 16 (2024) 8772–8782.
[35] J.R. Li, N. Li, L.L. He, J. He, Chin. Chem. Lett. 36 (2025) 109934.
[36] J.L. Shi, R.F. Chen, H.M. Hao, et al., Angew. Chem. Int. Ed. 59 (2020) 9088–9093.
[37] X.Y. Yan, B.B. Wang, J. Ren, et al., Angew. Chem. Int. Ed. 61 (2022) e202209583.
[38] J.M. Seo, H.J. Noh, H.Y. Jeong, J.B. Baek, J. Am. Chem. Soc. 141 (2019) 11786–11790.
[39] F. Haase, E. Troschke, G. Savasci, et al., Nat. Commun. 9 (2018) 2600.
[40] R. Paul, S.C. Shit, H. Mandal, et al., ACS Appl. Nano Mater. 4 (2021) 11732–11742.
[41] X. Ding, T.Y. Wang, B.Q. Yu, et al., Adv. Funct. Mater. 35 (2025) 202422291.
[42] L.L. Zheng, L. Tian, L.S. Zhang, et al., ACS Catal. 14 (2024) 2134–2143.
[43] K. Xiong, X.K. Jia, Y.X. Kong, et al., Adv. Funct. Mater. 35 (2025) 2510257.
[44] W.J. Xu, B.X. Huang, G.L. Li, et al., ACS Catal. 13 (2023) 5723–5732.
[45] Y.S. Bi, R.Z. Zhang, K.K. Niu, et al., Chin. Chem. Lett. 36 (2025) 110311.
[46] Y.H. Hou, P. Zhou, F.Y. Liu, et al., Nat. Commun. 15 (2024) 7350.
[47] J.L. Chen, S.C. Yan, F.T. Wang, et al., Angew. Chem. Int. Ed. 64 (2025) e202500924.